Dynamic simulation of the inflation gas of a tire under operational conditions

Axel Gallrein, Manfred Bäcker, Francesco Calabrese

Fraunhofer-Institut für Techno-
und Wirtschaftsmathematik ITWM
Fraunhofer-Platz 1, 67663 Kaiserslautern,
Germany
[axel.gallrein, manfred.baecker,
francesco.calabrese]@itwm.fraunhofer.de

Abstract

In this work, we are describing the coupling of an already existing tire model with a quasi-1D flow model to describe the inflation gas cavity fluctuations in a simple physical way. Since the gas cavity fluctuations are due to excitations - produced by transient tire deformations based on the interaction with the road surface - the gas model must be built to fully account for the tire shape variation. Thus, we derive the 1D Euler equations in a torus having a time and spatial dependent cross section area. The equations are discretized with a finite difference spatial discretization and integrated by an extended Lax-Wendroff scheme, which can handle source terms.

The coupling between the mechanical response and the inflation gas model is done in the following way: The transient shape of the tire appears as a source term in the Euler equations. The local gas cavity fluctuations on the other act on the tire structure and on the rim, both of which produce entries into the resulting spindle forces.

We are showing results for the overall non-linear model for transient simulations (cleat runs) and are comparing the results with and without dynamic gas cavity model and with measurements.

Finally, we showing how the overall model can be linearized around a steady state. With the resulting linear model, a modal analysis can be performed and we identify the so called 'cavity mode' and its dependence on rotational velocity.

Keywords: multibody dynamics, tire model, cavity model, linearization, NVH

1.Introduction

In the virtual development process, assessment and optimization of vehicle suspension and chassis performance are based on the forces that are transferred by the tire from road into the suspension. In this load transfer, the tire is one of the most critical components because the tire has a strong nonlinear behavior and is very difficult to model.

ITWM's tire model CDTire supports engineers in almost all analysis scenarios used in modern vehicle development processes from within modern multi body simulation (MBS) tools [1,2,5]. Special focus on tire belt dynamics and interaction with 3D road surfaces accurately captures the vibrations in both amplitude and frequency behavior.

The CDTire/3D is structural 3D shell based bead-to-bead model with sidewalls and belt that separately models all functional layers of a modern tire [5]. In this model, the inflation pressure is modeled as a uniform stress acting normal to the shell's faces. The pressure can vary depending on the application: prescribed by the MBS-tool to align to a constant pressure specified for a vehicle or scenario, but it can also be modified dynamically to simulate e.g. a sudden pressure loss in a tire. The authors have also show in previous publications that the pressure dependency is modeled physical correct.

For many applications, this description of the inflation pressure as a time dependent quantity is sufficient. However, there are tire applications where it is needed to describe the inflation gas using a dynamic gas equation (Euler or Navier-Stokes). One such example is when the tire model is used in NVH (Noise-Vibration-Harshness) applications where the frequency range extends the 250 Hz range. For passenger car tires, a first mode of the inflation gas is at around 200 Hz to 240 Hz, depending on tire size. This mode couples with the tire structure and rim and yields significant peaks in the spindle force spectrum, which have to be considered in the NVH assessment of a car.

In this paper, we are modeling the inflation gas of a tire by an isentropic compressible Euler equation and couple it to the tire dynamics in the nonlinear transient application range. After validation of the overall model by comparison with respective measurements, the authors are also describing how one can derive a linear model from the overall transient tire model, which can be used in linear FEM based NVH-tools.

It should be pointed out that the tire rotation will yield a split in the aforementioned cavity mode (which increases with rotational velocity) which is shown at the end of this paper.

2. Tire model

In this chapter, we sketch the modelling concepts of CDTire/3D, which has been used to include the gas cavity model as a compressible Euler cavity model.

The basic concept of this modeling approach is that the local deformation behavior of a real tire should be identically observed in the MBD tire model. This leads to the requirement that the model must have a detailed materialized shell representation of sidewall and belt to feature the deformation behavior of the load bearing structure. With this requirement, one can correctly feature both in-plane and out-of-plane (transversal or lateral) deformation behavior. The density properties of the shell are represented by node masses with 3 degrees of freedom, spanning the load bearing surface. Figure 1 shows a typical discretization:
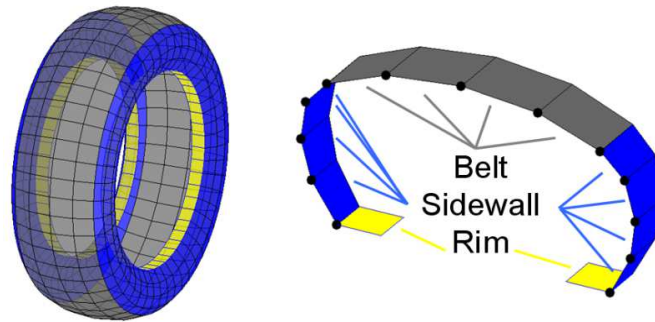
Figure 1: Node distribution of tire and cross section

The elastic properties of the shell are realized by an anisotropic elastic membrane part and adaptation of the Kirchhoff-Love hypothesis for bending. The bending is implemented around all circumferential and lateral edges, and around two diagonals of each cell. To constitute the bending laws, the 4-point cells will be divided into their elementary triangles. Bending of adjacent cells relative to the edge is split into bending of two pairs of triangles. The same is done for bending around diagonals of a cell. Figure 2 shows this principle and the finite difference properties of this approach:
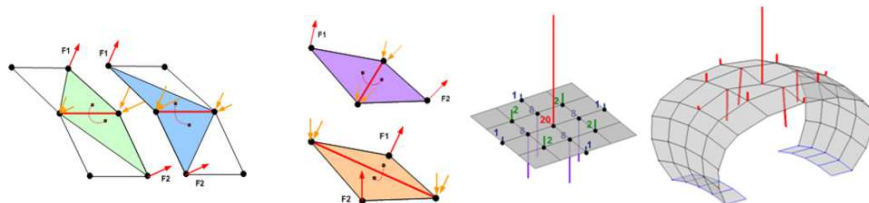
Figure 2: Triangle pairs used for cell edge bending and around diagonals of a cell (left two), finite difference stencil of isotropic bending and non-linear reaction forces of center belt node radial unit displacement

The anisotropy of the tire is a direct consequence of the tire structure. The physical tire is built from different component layers like inner liner, carcass, steel belt layers, cap plies, tread etc., with most of these being reinforced by synthetic cords or steel wires. Each reinforcement layer introduces a materially preferred direction. All the characteristic component layers described above have a separate representation in the model. The main advantage of this description is that the model is completely configurable. One can, for example model an arbitrary number of steel belt layers. Every steel belt layer can have a specific belt angle and specific local stiffness properties. This is important for the modeling of truck tires, which can have a varying number of steel belt layers and varying angles compared to passenger car tires. In a final pre-processing step, these layers are condensed into one shell representation. Figure 3 shows this layering approach:

Figure 3: Functional component layers of the tire

For more details on this modeling approach, we refer to [5].

3. Cavity model

From the different sources of interior and external vehicle noise, the cavity mode is probably the less understood. This is partially due to the existence of complex interactions phenomena between the road and the tire. The development of numerical models which allows predicting this effect is very important for the product design development but a non-trivial task.

In the literature, several one dimensional models have been proposed to predict the cavity resonance frequency based on some assumptions about the deflected geometry of the tire. Thompson [7] were able to identify the fundamental acoustic resonance peak by expressing the 1D wave equation into a torus. Further works focused Finite Elements models to numerically investigate the road-tire interactions. However, detailed Finite Elements Methods lead to a long computational times and the coupling of gas flow model with less time consuming tire models based on some ring models has been less investigated.

In this work, we first generalize the approach initially proposed by Thompson to describe the 1D gas flow in a torus in order to fully account for the influence of cross-sectional variation, based on rolling a deflected tire, on the gas flow properties and describing equations. To achieve that, we derive the Euler equations on a spatial and time dependent torus. No additional hypothesis about the variation of the shape will be postulated.

Mainly by studying the work of Bourdarias &Gerbi [3] we derived the following equation for the deformable tire torus cavity:

$$
\begin{aligned}
\partial_t(\rho A) + \frac{1}{R}\partial_\varphi(\rho A v) &= 0 \\
\partial_t(\rho A v) + \frac{1}{R}\partial_\varphi(\rho A v^2 + p A) &= p\frac{1}{R}\partial_\varphi A
\end{aligned}
\tag{1}
$$

In (1), $\rho = \rho(\varphi, t)$ is the local density of the inflation gas, $v = v(\varphi, t)$ is the local flow velocity, $A = A(\varphi, t)$ is the local cross section area of the tire tube and $p = p(\rho)$ is the local pressure as a function of the local density.
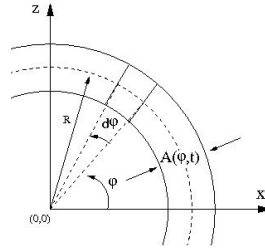
Figure 4: Volume element in torus coordinate system

If the cross section area of the tire tube would be constant in spatial coordinate φ and in time t, the source term on the right side of the equation (1) would be zero and we would have the standard homogenous Euler equation on a torus.

If we introduce the abbreviations $\alpha = \rho A$ and $\mu = \rho A v$ and prescribe a functional dependence of the pressure on the density $p(\rho) = c^2 \rho$ and re-write this as $p(\alpha) = c^2 \frac{\alpha}{A}$, equation (1) can be re-written as equation (2) in conservation form:

$$
\begin{aligned}
\partial_t\alpha + \frac{1}{R}\partial_\varphi\mu &= 0 \\
\partial_t\mu + \frac{1}{R}\partial_\varphi\left(\frac{\mu^2}{\alpha} + c^2\alpha\right) &= c^2\alpha\frac{1}{R}\frac{\partial_\varphi A}{A}
\end{aligned}
\tag{2}
$$

A second advantage of this transformation is that now the dependency of A is formally only in the source term on the right hand side of the second equation and there is no time derivative in the source term.

We are solving equation (2) by using an extended Lax-Wendroff scheme in which for the homogeneous part the discrete Lax-Wendroff scheme will be used and for the source term a second order approximation in time.

4. Coupling of structural tire model and cavity model

For the coupling of the structural tire model with the cavity model, there is the problem that the underlying physical regimes have different time scales for the dynamic response. From a numerical point of view, the two regimes would be time-integrated by different time step sizes. If we consider a typical passenger car tire, the step size to integrate the Euler equation of the gas cavity - taking into account the Courant-Friedrichs-Lewy condition (CFL) - is expected to be smaller than the step size typically used to integrate the structural tire model.

Considering this, we set up the overall integration scheme by an embedded co-simulation, in which the structural tire model is the master. To integrate the structural tire model with an explicit Newmark method, a dedicated variable step-size control is used. This scheme is sketched in Figure 5:
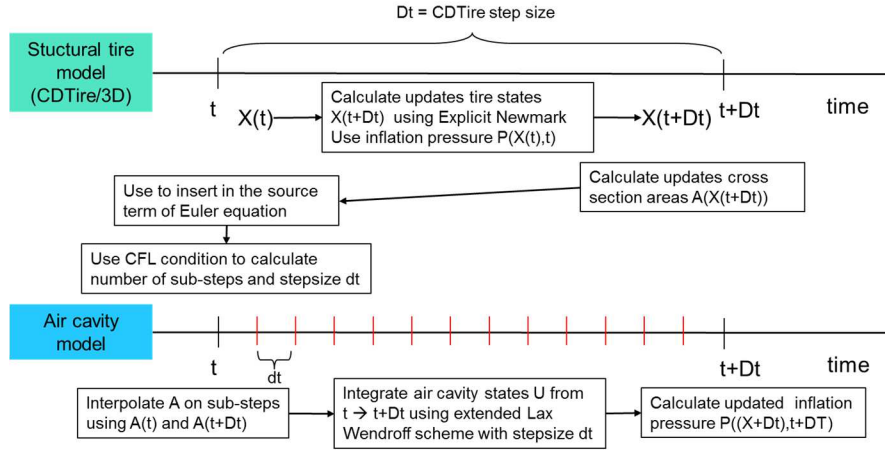

Figure 5: Co-simulation time integration scheme

Finally, the overall tire model including gas cavity model is embedded in the integration scheme of the MBS tool where the vehicle model is integrated. Because the typical step size of the vehicle simulation is usually bigger than the step size of the tire model, a similar co-simulation scheme is used between MBS master and structural tire model. The non-linear, transient results shown in Chapter 6 have a dedicated stand-alone driver software acting as MBS master.

5. Linearization around steady state rolling

Applying finite difference discretization on all spatial derivatives, the non-linear (discretized) tire and (discretized) cavity model can be abbreviated by (3), where the first equation is the combined kinematical and dynamical equation of the rim plus tire, with x as positional and velocity state and E containing the mass matrix of rim and (discretized) tire states. Also, f denotes both the forces acting on rim and tire as well as the first order kinematical equations. Furthermore, z is the (discretized) first order state of the cavity model (both mass and momentum) and g denotes the right hand side of the spatially discretized rhs of the compressible Euler equation.

$$\begin{aligned} E\,\dot{x} &= f(x,z) \\ \dot{z} &= g(x,z) \end{aligned} \qquad (3)$$

For the linearization, a method similar to the so called ALE (Arbitrary Lagrangian Eulerian) method has been used (see also [4,6] for a discussion on such methods). In this method, the stationary rolling tire is described in a special spatial description instead of a material description. An important result in this method is the rise of gyroscopic forces acting on the tire explicitly in the equation of motion (3). This is needed to introduce the correct velocity dependent modal behavior into the linear system. The same mechanism is performed on the compressible Euler equation. Formally, this introduces an additional parameter ω, the angular velocity of the rim around the rotating axis of the rim. It has to be pointed out that the linearization is performed around a 'steady state', with all degrees of freedom (dof) of the rim kinematically constraint, except for the rim rotation (see [5] for more detail). The new functions $\bar{f}, \bar{g}$ contain the gyroscopic forces due to ω, and $\bar{f}$ contains additionally the inverted matrix E.

$$\begin{aligned} \dot{x} &= \bar{f}(x,z;\omega) \\ \dot{z} &= \bar{g}(x,z;\omega) \end{aligned} \qquad (4)$$

Linearization yields

$$\dot{s} = A(\omega)\,s, \qquad (5)$$

with A containing the respective jacobians of $\bar{f}, \bar{g}$ and s containing x, z. Solving the eigenvalue problem (EVP) that arises from (5), eigenvalues (mode frequencies and damping) and eigenvectors (mode shapes) can be analyzed. In the following we show numerical examples of a typical 225/45 R 17 tire with an inflation pressure of 2.5 bar. Figure 6 shows typical 'radial' modes of the non-deflected, non-rotating tire, where the deformation is mainly in radial direction.
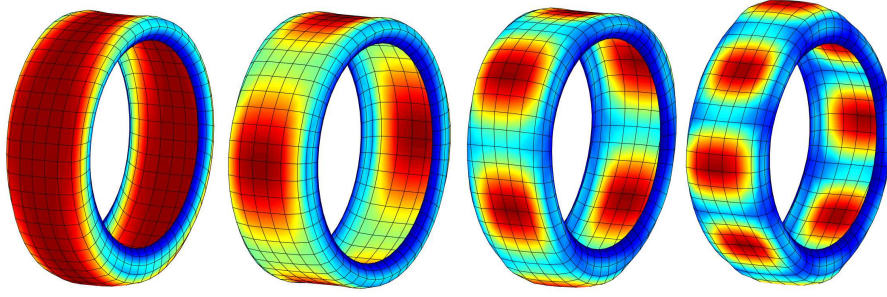
Figure 6: Radial tire modes R1 (76 Hz), R2 (97 Hz), R3 (120 Hz), R4 (146 Hz)

Figure 7 shows typical 'lateral' modes of the non-deflected, non-rotating tire, but they contain also significant amounts of radial and torsional deformations.
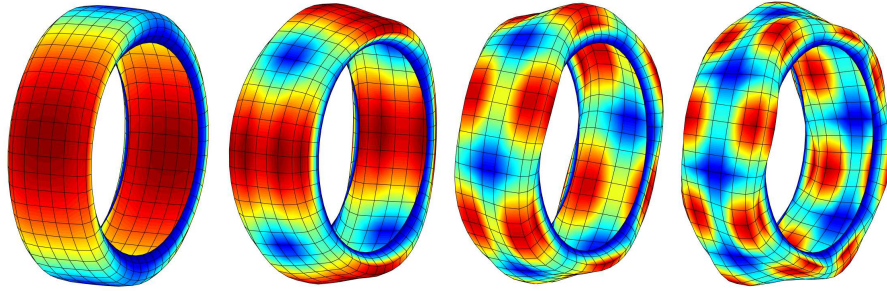

Figure 7: Lateral tire modes L1 (59 Hz), L2 (101 Hz), L3 (145 Hz), L4 (174 Hz)

It must be pointed out that including the rotational effects adds significant asymmetry to the matrices. As such, the resulting EVP is a complex EVP with complex modes and frequencies. Visualization of the modes was performed by extracting the positional part of $\frac{1}{2}(x + \bar{x})e^{i\omega t}$, for some t with ω as the imaginary part of the respective eigenvalue. Also, the inclusion of the compressible Euler cavity model introduces zero modes, as the inflation gas is rotationally unconstraint (periodic boundary conditions).

6. Results

In the following we show results of a 225/45 R 17 tire with an inflation pressure of 2.5 bar in various scenarios. If not stated specifically different, it is always the same tire at the same inflation pressure (initially).

Figure 8 compares the simulation results of the constant (prescribed) pressure cavity model against the ideal gas cavity model, the compressible Euler cavity model and the measurement. In this test, the tire is deflected (very slowly with 5..10 mm/s deflection velocity) against a rigid, flat surface and the corresponding vertical force is measured. While the tire is first deflected and then slowly unloaded - yielding a significant hysteresis - the simulations are performed only with progressive deflection, as the progressive deflection part is invariant (at these very slow deflection velocities) against range and velocity changes. The unloading part featuring the hysteresis does depend on range and velocity and is ignored here. The sudden non-linearity at around 17000 N preload is the start of the 'tire ground out', when the tire is deflected so much that the tire bead region starts to have internal contact with the tire innerliner at the shoulder.
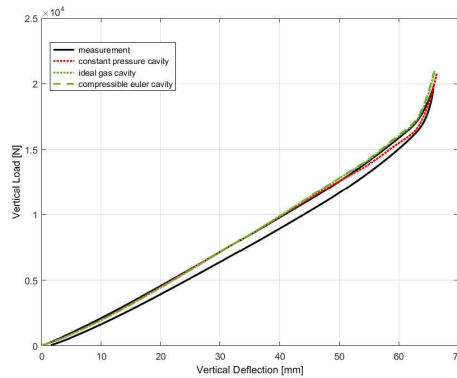

Figure 8: Vertical load/deflection measurement against 3 cavity models

While below 10000 N preload, all cavity models yield the same result, starting from 10000 N preload and significantly starting from 15000 N preload, the constant pressure cavity model underestimates the vertical

stiffness, while both ideal gas and compressible Euler cavity model correctly capture the increase in inflation pressure due to the changing (decreasing) inflation gas volume. The results for the ideal gas and compressible Euler cavity model correctly yield virtually identical results, as the quasi-static character of this experiment does not introduce significant dynamics. As a first result, this shows that the inclusion of a cavity model can improve the accuracy of the overall model's predictive capabilities – even for quasi-static scenarios.

As a further step, we analyze a transient scenario: the cleat run experiment. In such an experiment, the tire is deflected to a prescribed preload (typically onto a rotating drum) and the vertical displacement capability of the test rig is then mechanically fixed to prevent any dynamics other than rim rotation and tire dynamics. The velocity of the surface (typically a drum rotation) is then increased to a prescribed value. The surface is smooth except for mounted obstacle, typically a chamfered rectangular cleat (with at least the width of the tire) in either 90° or 45 ° orientation relative to the forward direction. While the tire repeatedly hits the obstacle, the resulting spindle forces are measured. This effectively tests the transfer behavior of the tire from road excitation to spindle forces. Figure 9 shows the schematic setup of a cleat run experiment:
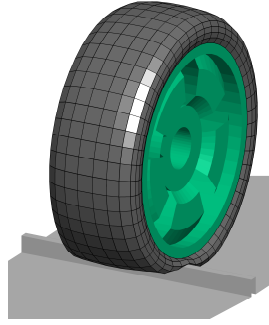

Figure 9: Schematic setup of a cleat run experiment

As the tire needs an inflation gas for sensible operation, the only way to prove the influence of the inflation gas on the measurement is to change the properties of the inflation gas while the tire and the operating conditions remain identical, including the inflation gas pressure. Figure 10 compares the 90° cleat run measurements (rectangular shape, 10 mm height, 20 mm width) of a tire mounted on a 19'' rim filled with air as well as helium, both at 2.5 bar for 3 preloads (3000 N, 5000 N, 7000 N) and 3 velocities (20 km/h, 60 km/h, 90 km/h) on drum:
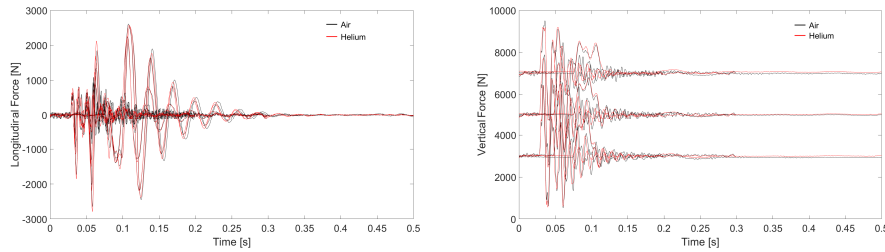

Figure 10: Longitudinal (left) and vertical (right) spindle force of air and helium filled tire on 19'' rim

The above pictures are only meant to demonstrate the transient character of the experiment. However, analyzing these measurements in frequency domain yields some interesting insights. Figure 11 shows the same measurements as FFT signals in frequency domain:
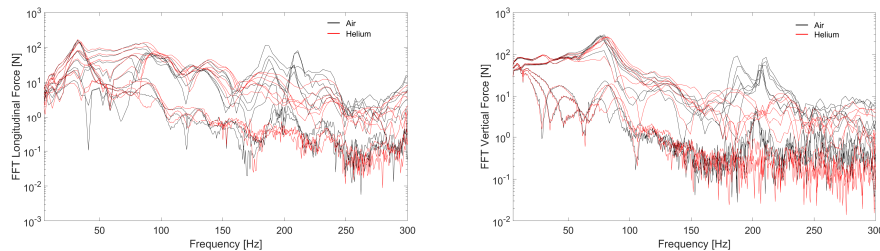

Figure 11: Longitudinal (left) and vertical (right) spindle force FFT of air and helium filled tire on 19'' rim

The most striking difference between air and helium filled tire response is at around 200 Hz. The air filled tire displays peak(s) that the helium filled tire does not. These frequencies can be explained by a resonant vibration of the inflation gas within the tire cavity, hence the name 'cavity mode'. A rough estimate of this frequency can be obtained by the formula $f = \frac{c}{2\pi R}$, where c is the speed of sound and R is radius of the gas column. For a tire mounted on a 19'' rim, a good estimate of the tire cavity radius is 0.28 m. With the speed of sound of 343 m/s of air at 20° Celcius, the cavity frequency is 195 Hz. With the speed of sound of 981 m/s of helium at 20° Celcius,

the cavity frequency is 558 Hz, which is well outside the resolution of the test rig equipment. Of course, some of the measurements feature 2 distinct peaks, which are due to the splitting of the cavity mode as a result of rotation and this will be explained later.

A secondary difference at closer inspection is a slight shift of the main frequencies (30 Hz longitudinal and 75 Hz vertical force response) with a clear tendency to increasing the frequency for the helium filled tire. This can be explained by interpreting the sound velocity as a measure of a 'stiffness' in series between tire and rim. An increase in sound velocity increases this 'stiffness' and as a result the frequency. In fact, the ideal gas cavity model may be interpreted as a gas with infinite 'stiffness'.

We now continue our comparison of the 3 cavity models of the 225/45 R 17 tire. A good estimate of the radius of the air column is 0.24 m, which yields an estimated cavity frequency of 227 Hz. Figure 12 compares the 3 cavity models against a 90° cleat run measurement (rectangular shape, 20 mm height, 20 mm width) at 2400 N preload, 2.5 bar and for 30, 60, 90 km/h in frequency domain (PSD) on a drum surface:
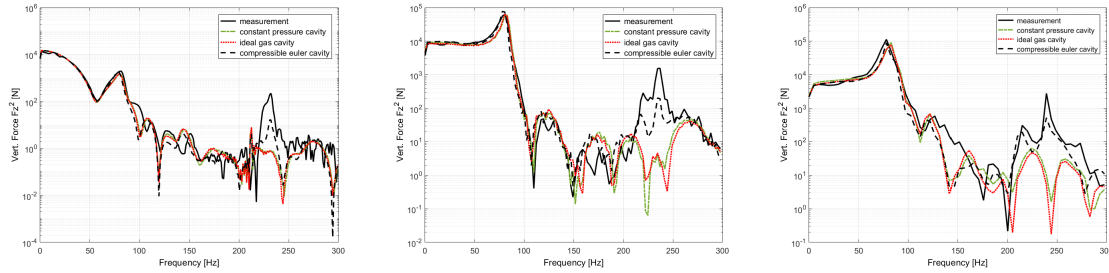

Figure 12: 90° cleat run vertical force PSD's at 30 (left), 60 (middle) and 90 (right) km/h against 3 cavity models

The measurements again show the cavity mode behavior at around 225 Hz. While it is (almost) a singular peak for 30 km/h, this peak splits into 2 peaks at 60 km/h and 90 km/h with the split at 90 km/h being significantly larger. This indicates that the split is a direct function of the velocity. An explanation for this behavior will be discussed later. The only cavity model that can capture this behavior is the compressed Euler cavity model. Both constant pressure cavity model and ideal gas cavity model fail to feature the force response amplitude at the cavity frequency range. This means that in order to extend the frequency behavior prediction capability beyond 200 Hz, the compressible Euler cavity model is needed. As a secondary remark, both constant pressure cavity model and ideal gas cavity model show an increase in the main frequency at ~80 Hz, which is due to the infinite 'stiffness' of these cavity models.

Interestingly, a split in cavity mode frequency due to the tire's deformation is not featured in the vertical force response. Figure 13 compares the 3 cavity models against a 90° cleat run measurement (rectangular shape, 20 mm height, 20 mm width) at 30 km/h velocity, 2.5 bar and for 2400, 4800, 7200 N preload in frequency domain (PSD) on a drum surface:
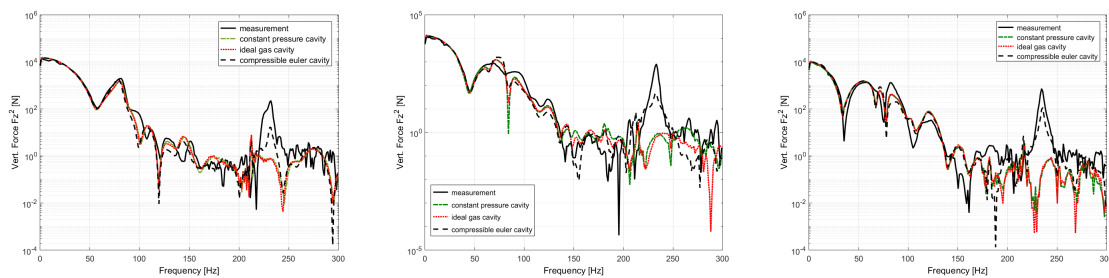

Figure 13: 90° cleat run vertical force PSD's at 2400 (left), 4800 and 7200 (right) N against 3 cavity models

For a better understanding, we move to the results of the linearization. Figure 14 shows the mode frequency over the mode number of the structural modes of the tire with constant pressure cavity model and with compressible Euler cavity model. It must be pointed out that the compressible Euler cavity model yields additional modes that the constant pressure cavity model does not: zero modes of the circumferentially unbounded (periodic boundary conditions) cavity states and the cavity modes itself. For the non-deflected, non-rotating and rim fixed wheel, the cavity mode frequency here is 226 Hz. For the sake of comparison, these additional modes were eliminated from the following mode numbering, so that the rest can be easily compared. The cavity modes can be easily identified by a very small real part of the eigenvalue (small damping). The eigenvalues with negative imaginary part (negative frequency) are shown as positive frequencies (conjugate complex eigenvalue) and the real part (damping) is not shown here. However, the sorting is done by 'smallest magnitude', so the damping does have an impact on the numbering.
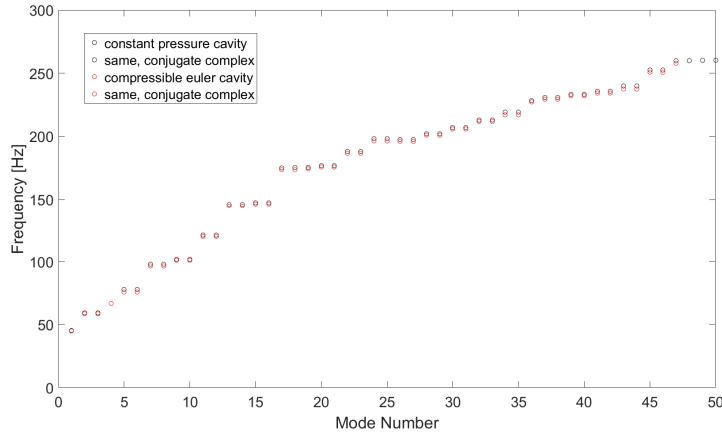
Figure 14: Modal frequencies of non-deflected, non-rotating, rim-fixed wheel (without cavity modes)

The conjugate complex modes for this scenario have identical absolute frequency and damping values, resulting in double entries for each mode number. As they have identical absolute frequency, this is not visible. Many modes show up as 2 mode number pairs; these are the modes that have a second linear independent mode shape (same shape but with a different beginning angle around the rotational axis), but this does not hold for all modes. E.g., mode 1 (L0, constant lateral deformation) or mode 4 (C0, constant circumferential deformation) are unique modes (apart from conjugate complex) as any rotation of the shape around the rotational axis yields the same shape. Interestingly, these 2 modes feature almost no difference between the cavity models as the volume change for these modes is zero (or very small). Otherwise, the compressible Euler cavity model reduces the frequency of the corresponding mode of the constant pressure cavity model. This also explains nicely the effect main frequency reduction of the main frequency for the non-linear, transient model in Figure 12: the associated mode has a lower modal frequency due to the coupling with the compressible Euler cavity model.

Figure 15 compares the modal frequencies obtained with the compressible Euler cavity model for the non-deflected, rim-fixed wheel at rotational velocities corresponding to 0, 10, 20, 30 m/s. As explained in [1,2,4,6], the gyroscopic effects yield a split in frequency (kind of Doppler's effect) with increasing velocity. However, that means that in Figure 15, the ordering of mode numbers ('smallest magnitude') yields a possible switch of shapes, meaning the mode shapes at a certain mode number may not be the same (and generally aren't).
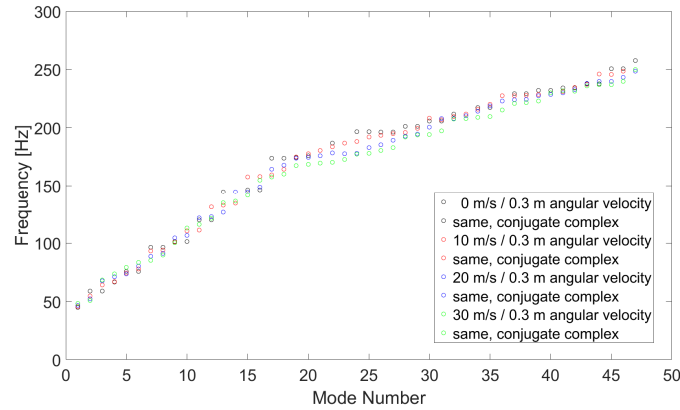

Figure 15: Modal frequencies of non-deflected, rim-fixed wheel (without cavity modes) at 0, 10, 20, 30 m/s

The frequency split due to gyroscopic effects eliminates the 'pair wise' ordering of certain modes. An in-depth analysis of the split per mode shape is worth investigating, but not performed here. But this depiction makes one important fact clear: there is no monotone dependence of frequency content on velocity. At certain modes (or frequency ranges) the higher velocity may have larger content, at others smaller or vice-versa.

Lastly, Figure 16 looks at the split due to rotation for the cavity modes (ignoring the zero modes):
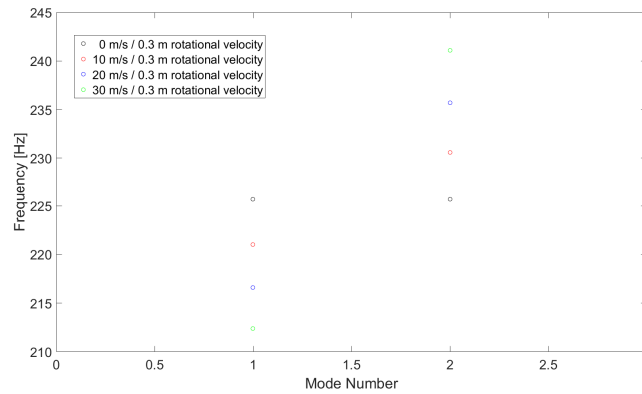
Figure 16: Modal cavity frequencies of non-deflected, rim-fixed wheel at 0, 10, 20, 30 m/s

This is a clear message: the split due to rotation of the cavity modes of the non-deflected tire is a linear function of the rotational velocity. It also fits nicely with the split in vertical force frequency of the non-linear, transient tire and cavity model during cleat runs.

7. Conclusion

The authors have shown how to extend an existing structural tire model with a dynamic gas cavity model. The gas cavity model has been modeled by a 1D non-linear Euler equation with a source term representing the effect that the cross section of the gas cavity can vary in space and time. Projected to the tire the cross section variation is representing the tire deformation due to rolling and dynamical loading running for example over an uneven road.

Additionally, the coupling of both physical systems, the structural tire model and the inflation gas cavity model has been discussed.

From the overall non-linear model, the authors have sketched a method to derive a linear model of the tire around a steady state.

Results and respective correlation to measurements have been shown for the transient model and for the derived linear model.

For the transient model we simulated a cleat run experiment on a drum test rig and compared this to related measurement. It could be successfully shown that the tire model with dynamic gas cavity covers all qualitative effects of the so-called cavity mode and fits to the measurements also quantitatively in an impressive way. It could also be shown that the inclusion of the dynamic gas cavity model improves the overall accuracy of the tire model for example in the vertical stiffness behavior for very high preloads, but also in the frequency responses for typical tire modes far under the cavity frequency.

Using the derived linear model a modal analysis have been performed and the results have been discussed with a focus on rotational velocity.

As a perspective, the authors are currently working on an equivalent second order formulation of the gas cavity model which allows to export the overall linear model as a second order MCK system, which can be imported in FEM based NVH tools like Nastran.

Acknowledgments

References

[1] M. Baecker, A. Gallrein, M. Roller: Noise, vibration, harshness model of a rotating tyre, Vehicle System Dynamics Vol.54 – Issue 4, pp. 474-491, 2016, doi: 10.1080/00423114.2016.1158844, http://dx.doi.org/10.1080/00423114.2016.1158844

[2] M. Baecker, A. Gallrein, M. Roller: From Road Excitation to Spindle Forces in Frequency Domain: Linearization of the Rolling Tire, SAE Technical Paper 2015-01-0625, 2015, doi:10.4271/2015-01-0625.

[3] C. Bourdarias, S. Gerbi: A conservative model for unsteady flows in deformable closed pipes and its implicit second-order finite volume discretisation, Computers & Fluids, Vol.37 – Issue 10, pp. 1225-1237, 2008,

https://doi.org/10.1016/j.compfluid.2007.09.007

[4] M. Brinkmeier, U. Nackenhorst: An approach for large-scale gyroscopic eigenvalue problems with application to high-frequency response of rolling tires, Comput. Mech. (2008) 41/4: 503-515, DOI 10.1007/s00466-007-0206-6.

[5] A. Gallrein, M. Baecker, A. Gizatullin: Structural MBD Tire Models: Closing the Gap to Structural Analysis - History and Future of Parameter Identification, SAE Technical Paper 2013-01-0630, 2013, doi:10.4271/2013-01-0630.

[6] I. Lopez, R. Blom, N. Roozen, H. Nijmeijer: Modelling vibrations on deformed rolling tires - a modal approach, Journal of Sound and Vibration, 307(3-5), 481-494. DOI 10.1016/j.jsv.2007.05.056.

[7] J. K. Thompson: Plane Wave Resonance in the Tire Air Cavity as a Vehicle Interior Noise Source, Tire Science and Technology: January 1995, Vol. 23, No. 1, pp. 2-10 , doi: http://dx.doi.org/10.2346/1.2137495